

ARTICLE OPEN



The influence of the Asian summer monsoon on volcanic aerosol transport in the UTLS region

Xue Wu^{1,2}, Qi Qiao³, Bing Chen^{3✉}, Xin Wang^{1,2✉}, Lars Hoffmann⁴, Sabine Griessbach⁴, Yufang Tian^{1,2} and Yinan Wang^{1,2}

This study analyses the influence of the Asian summer monsoon on volcanic aerosol transport. Realistic, altitude-resolved SO₂ emissions of a middle-latitude volcanic eruption (Sarychev 2009) and a tropical volcanic eruption (Nabro 2011) were retrieved and used to initialize the simulations of the long-range transport and dispersion of the sulfate aerosol plumes. The barrier effect of the Asian summer monsoon anticyclone (ASMA) isolated the Sarychev eruption plume outside of the ASMA but constrained the Nabro eruption plume inside of the ASMA, which is most evident in the UTLS region between isotropic surfaces of 360–420 K. Meanwhile, the ASMA could transport a fraction of the plume outside of ASMA quasi-horizontally to the tropical tropopause layer along the southeastern periphery of the anticyclonic circulation, and lift the volcanic plume inside the ASMA anticyclonically across the tropopause with an ascent rate of approximately 0.8 K/day. By enhancing the meridional transport in the UTLS region and lifting volcanic aerosols across the tropopause, the ASMA significantly expanded the potential effects of volcanic eruptions.

npj *Climate and Atmospheric Science* (2023)6:11; <https://doi.org/10.1038/s41612-023-00339-w>

INTRODUCTION

The regional and global climate impacts of volcanic aerosols in the upper troposphere/lower stratosphere (UTLS) have received great attention. Although there have been few large volcanic eruptions in recent decades, small and medium volcanic eruptions have continuously increased stratospheric aerosol levels. The sulfate aerosol from volcanism has become a significant source of aerosols in the tropical UTLS^{1,2}. For instance, recent small and medium-sized volcanic eruptions, such as Kasatochi (2008), Sarychev (2009), and Raikoke (2019) in the extratropics and Nabro (2011) and Ulawun (2019) in the tropics, have enhanced stratospheric aerosol loading^{3–7} and have had a profound impact on the global aerosol optical depth of the stratosphere⁸. Other studies suggest that nonvolcanic aerosol particles, e.g., anthropogenic sulfur, black carbon, and organic carbon released at the Earth's surface, may also be a relevant source of the stratospheric aerosol layer^{9,10}. In that case, it is essential to accurately estimate the climate impacts of volcanic eruptions because the climate impact of anthropogenic greenhouse gases and aerosol particles could be better assessed if natural forcings, such as volcanic eruptions, are explicit.

The atmospheric background conditions, the amount of emitted SO₂, and the plume heights of volcanic eruptions are all essential parameters that directly determine the transport pathways of volcanic SO₂ and sulfate aerosols. Tropical volcanic eruptions may inject SO₂ and sulfate aerosols directly into the tropical tropopause layer (TTL). From the TTL, those sulfur emissions are transported upward by the ascending branch of the Brewer–Dobson circulation and then spread to the middle and high-latitude stratosphere. Although the sulfur emissions from volcanic eruptions in the middle and high latitudes may not directly enter the Brewer–Dobson circulation, they may take advantage of the extratropical Rossby wave breaking to transport sulfur from the extratropical UTLS to the TTL. The Asian summer

monsoon (ASM) is one of the essential transport mechanisms between the extratropical UTLS and the TTL in boreal summer^{11–13}. The ASM is featured with a strong anticyclonic circulation in the UTLS, the Asian summer monsoon anticyclone (ASMA), ranging from East Asia to the Middle East¹⁴. The ASMA can significantly increase transport between low and middle latitudes in the UTLS region. The persistent deep convection associated with the ASM may transport trace gases and aerosols from the atmospheric boundary layer upward into the UTLS^{15–20}. However, although the role of the ASM in atmospheric constituent transport and exchange is gradually recognized, the influence of the ASM on aerosol transport is still under investigation^{21,22}. One critical reason is that the limited spatial and temporal resolution of existing volcanic SO₂ observations and inventories fails to properly constrain realistic volcanic aerosol transport and dispersion.

In this study, we investigate the role of the ASM in transporting volcanic plumes in the UTLS region. High-resolution sulfur emissions retrieved for the two volcanic eruptions, the Sarychev eruption in June 2009 and the Nabro eruption in June 2011, are used as “realistic” tracers for transport studies. The Sarychev volcano (48.1°N and 153.2°E) is located northeast of the ASM. In contrast, the Nabro volcano (13.4°N and 41.7°E) is on the southwest edge of the ASM. These two volcanic eruptions distinguished by geographical locations and time are typical cases for investigating the influence of the ASM on volcanic aerosol transport between the tropics and extratropics inside and outside of the ASM.

RESULTS

Volcanic SO₂ emission time series

The time series of the altitude-resolved SO₂ injections from the Sarychev and Nabro eruptions are shown in Fig. 1. The Sarychev eruption started on 12 June 2009. The eruption continued for

¹Key Laboratory of Middle Atmosphere and Global Environment Observation, Institute of Atmospheric Physics, Chinese Academy of Sciences, Beijing, China. ²University of Chinese Academy of Sciences, Beijing, China. ³Key Laboratory of Atmospheric Environment and Processes in the Boundary Layer over the Low-Latitude Plateau Region, Department of Atmospheric Science, Yunnan University, Kunming, China. ⁴Jülich Supercomputing Centre, Forschungszentrum Jülich, Jülich, Germany.

✉email: chenbing@ynu.edu.cn; wangx2003@mail.iap.ac.cn

~5 days, and the SO₂ injections varied in height and magnitude. The most significant SO₂ injections were on 14–15 June between 10–18 km, and minor emissions followed until 16 June. Approximately 58% of the SO₂ (0.8 Tg) was injected into the lower stratosphere. For the Nabro eruption, the peak emissions were on 12 June 2011, 12 UTC to 13 June 2011, and 06 UTC at 14–18 km. Additional emissions occurred since 14 June 2011 and the peak emissions were at 7 and 11 km. In the first 2 days (12–13 June),

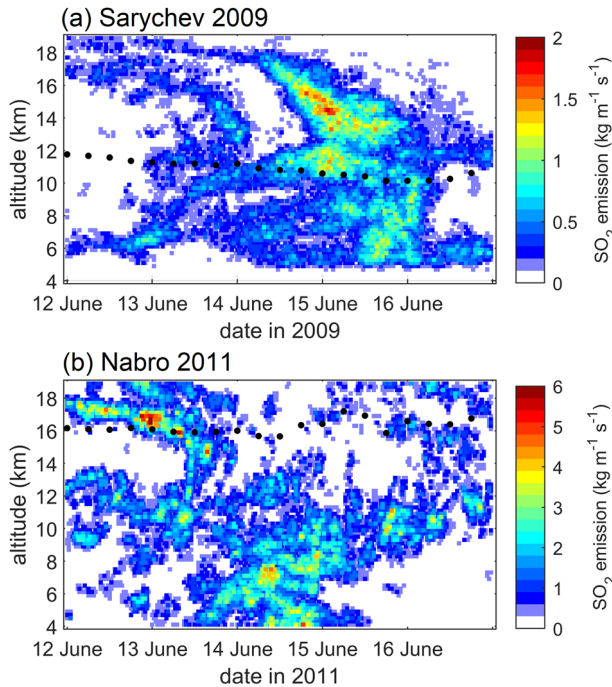


Fig. 1 SO₂ emission time series of two volcanic eruptions. **a** SO₂ emission time series of Sarychev eruption (2009) and **b** SO₂ emission time series of Nabro eruption (2011) (unit: kg m⁻¹ s⁻¹) derived from AIRS measurements using a backward trajectory approach (see texts in the Method section for details). The bin size is 15 min × 0.2 km. Black dots indicate the height of the tropopauses (based on the ERA5 reanalysis). Note that different color bar ranges are used in (a, b).

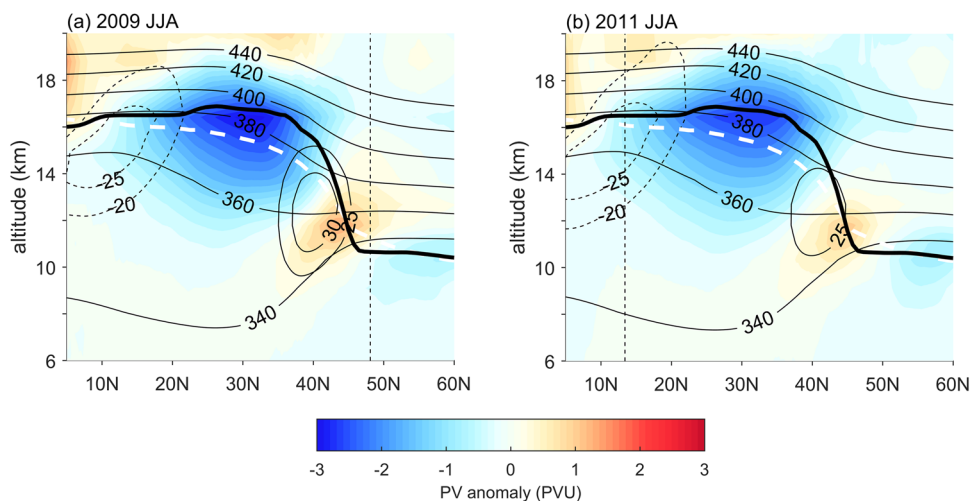


Fig. 2 Meteorological conditions in the ASMA (based on the ERA5 reanalyses). Potential vorticity (PV) anomaly (shaded, unit: PVU) in the approximate longitude range of the ASMA (40–120°E) for **a** 2009 (June–July–August) and **b** 2011 (June–July–August). The zonal wind is averaged between 40–120°E with solid black contours indicating the westerlies and dashed black contours indicating the easterlies. The dashed white line indicates the mean tropopause over 0–360°E, and the thick black line indicates the mean tropopause between 40–120°E. The thin black lines indicate the potential temperature. Vertical dashed lines mark the latitudes of the volcanoes.

most of the SO₂ (~55%) was injected directly into the lower stratosphere. About 26% of SO₂ (0.95 Tg) was injected into the lower stratosphere during the whole eruption period. The timelines of the two eruptions generally agree with the Global Volcanism Program reports^{23,24}, and the temporal development and plume heights of the two eruptions are consistent with more detailed studies^{25–28} too.

The volcanic SO₂ emission estimations with high altitude and temporal resolutions were used to initialize forward transport simulations. Based on the reconstructed SO₂ emissions, we assigned 100,000 air parcels for the Sarychev and Nabro eruption each. The total masses of SO₂ for the two cases were 1.4 Tg and 3.65 Tg, respectively. The SO₂ mass in each air parcel was uniform, but the number of air parcels at a specific time and altitude was proportional to the SO₂ emission rate at that time and altitude, as shown in Fig. 1. Then, the ERA-Interim wind field was used to drive the forward transport and dispersion simulations of the volcanic plumes. Forward trajectories were calculated with the MPTRAC model from the volcanoes' first eruption to 31 July 2009, 00 UTC for the Sarychev case, and 31 July 2011, 00 UTC for the Nabro case. During the trajectory simulations, the depletion of SO₂ was also simulated with hydroxyl chemistry, i.e., the chemical decomposition of SO₂ by hydroxyl radicals. We assumed that the sulfate aerosol converted from SO₂ remained in the volcanic plume in the UTLS region. The simulation outputs are given every three hours.

For conciseness, the evolutions of the volcanic SO₂ and the transport of the aerosol particles are evaluated by comparing with satellite observations in the Supplementary information.

The horizontal barrier effect of the ASMA

Figure 2 shows cross-sections of the ASMA in the boreal summers of 2009 and 2011. The ASMA is among the most prominent circulation patterns during summer in the Northern Hemisphere UTLS. It features an area of strongly negative potential vorticity (PV) anomalies because of its anticyclonic upper-level circulation, ranging approximately between the isentropic surfaces of 360–420 K, and it is also subject to dynamical variabilities²⁹. The northern part of the ASMA is bounded by subtropical westerlies. Moreover, the tropopause over the ASMA region is relatively higher than the zonal mean tropopause. With the long-range transport simulations, it is straightforward to see the ASMA circulation's influence on the volcanic plume's transport pathway.

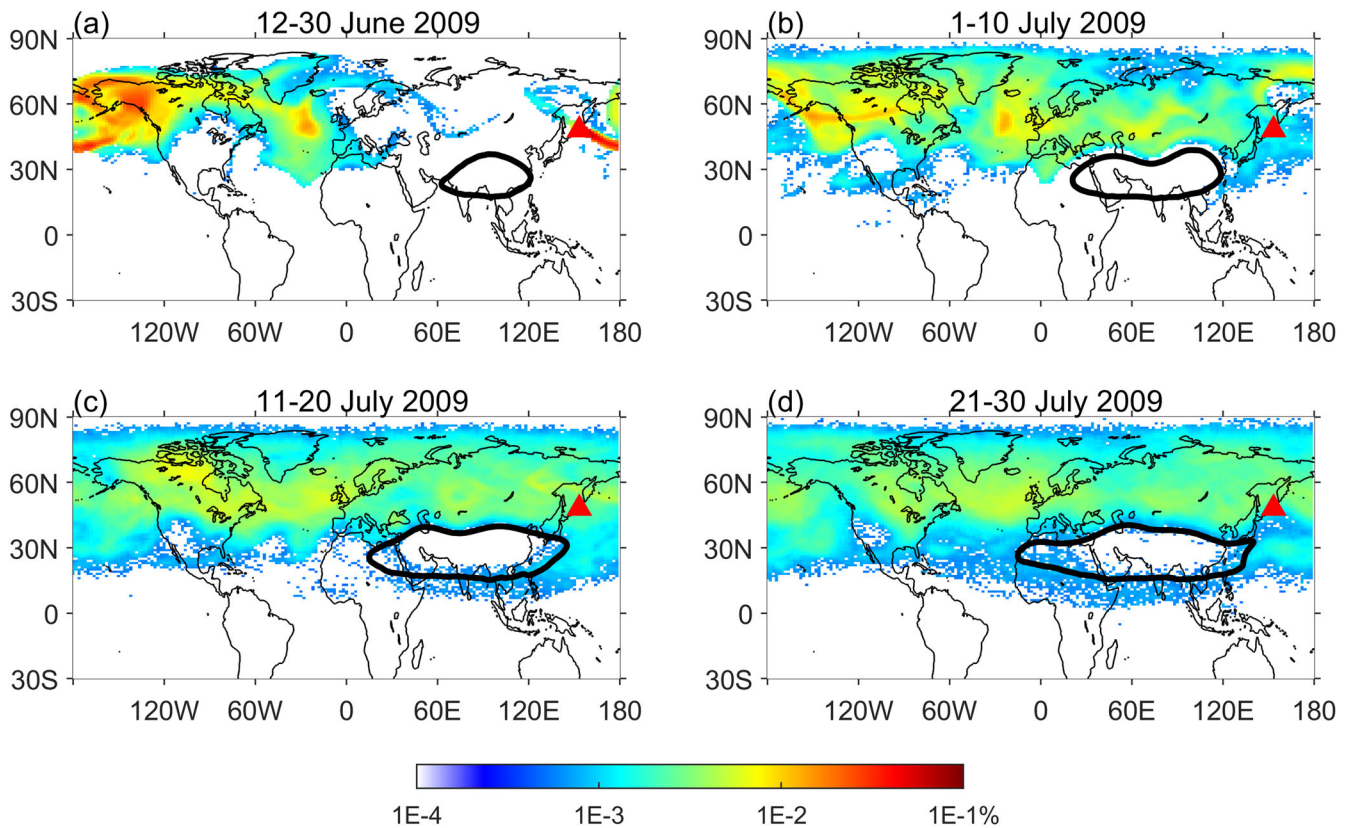


Fig. 3 Percentage (%) of air parcels between isentropic surfaces of 360–420 K from MPTTRAC simulations for the Sarychev eruption. The percentage of air parcels are shown during **a** 12–30 June 2009, **b** 1–10 July 2009, **c** 11–20 July 2009, and **d** 21–30 July 2009. The bin size is $2^\circ \times 1^\circ$. The boundary of the ASMA is marked by the 14,320 m geopotential height at the 150 hPa pressure level (thick black contours). The filled red triangles indicate the Sarychev volcano.

Figure 3 shows the distributions and evolution of the volcanic plume of the Sarychev eruption in the altitude range of the ASMA. The black contour is the geopotential height of 14,320 m on the pressure level of 150 hPa, which is commonly used as the boundary of the ASMA¹⁵. The color shading denotes the percentage of volcanic plume parcels in each $2^\circ \times 1^\circ$ bin to the total air parcels during the period of consideration. After the eruption, the volcanic plume generally dispersed eastward from 12 to 30 June 2009 and remained at middle and high latitudes (Fig. 3a). After another ten days (by 10 July 2009), a fraction of air parcels was dragged into the anticyclonic circulation of the ASMA transported toward the tropical UTLS, i.e., TTL (Fig. 3b). Later, more air parcels were entrained along the southern and eastern flank of the ASMA and spread toward the tropics (Fig. 3c, d). The barrier effect of the ASMA was more prominent as a hole of aerosol was formed after 10 July.

The transport of the Nabro eruption plume further demonstrated the barrier effect of the ASMA. As the Nabro volcano was located at the southwest edge of the ASMA in 2011, the volcanic plume was immediately wrapped into the anticyclone after the eruption and transported to higher latitudes in the Northern Hemisphere (Fig. 4a). Similar to previous studies^{29–32}, one important mechanism for air parcels escaping from the AMSA is the eastward-migrating anticyclones breaking off from the main anticyclone and the filaments separated on the northeastern and southwestern flanks of the anticyclone (Fig. 4b–d). The 14,320 m geopotential height contour over North America indicates the North American monsoon (NAM). The NAM occurs due to a similar mechanism as the ASM, i.e., the differences in thermal properties between land and ocean. The NAM plays a similar role as the ASM in Fig. 3, transporting aerosols from middle latitudes to lower

latitudes and isolating aerosols outside of the anticyclonic circulation, but it is much weaker in strength.

The ASM anticyclonic circulation generally promotes meridional transport as the subtropical jet retreats northward in boreal summer. The clear difference between the plume transport of the two volcanic eruptions is mainly due to the barrier effect of the ASMA, which is particularly obvious in the UTLS region.

Vertical transport of volcanic plumes in the convection region

To further investigate the volcanic plume transport pathway within the ASMA, we analyzed the forward trajectories of the Nabro eruption plume. The selected trajectories started from the SO_2 emissions in the upper troposphere between 12 and 16 June 2011 and ended at the lower stratosphere over the ASMA on 30 July 2011, as shown in Fig. 5. Figure 5a, b demonstrate the forward trajectories of five air parcels, colored by days since the starting date of the Nabro eruption to the end of the trajectory simulation and the potential temperature, respectively. Figure 5c, d demonstrate the corresponding vertical cross-sections.

The forward trajectories reflected the anticyclonic circulation of the ASMA. In the first 15 days, the volcanic plume circulated the ASMA along isentropic surfaces quasi-horizontally in the low and middle latitudes. The isentropic surfaces are tilted in the UTLS region, so the altitude of the plume vibrated between higher and lower altitude levels when circulating the ASMA. Afterward, while circulating anticyclonically, the plume slowly elevated across the tropopause due to diabatic heating, forming large-scale spiral trajectories over the ASMA. Figure 5e, f demonstrate the statistics of the potential temperature and altitude evolution of the trajectories. The potential temperature of the plume increased

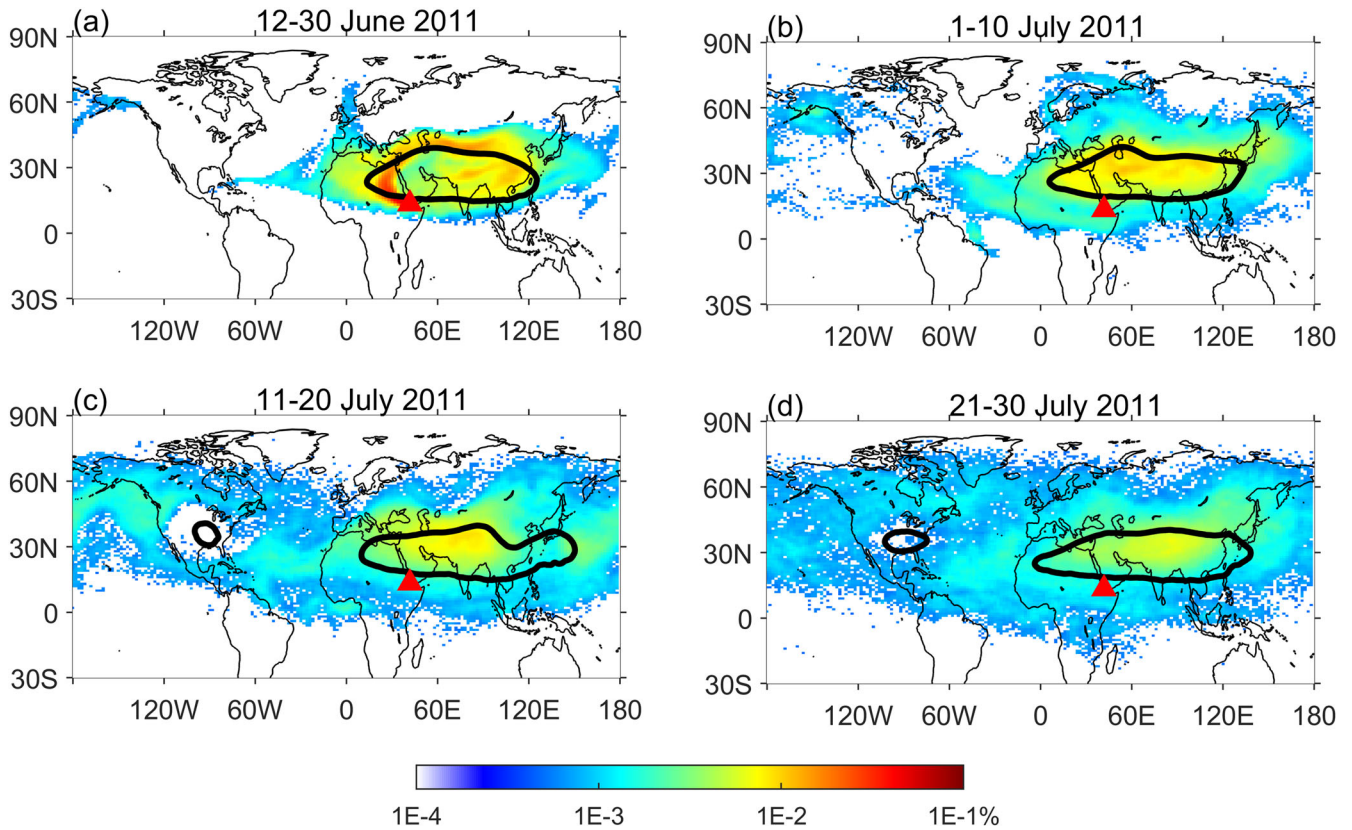


Fig. 4 Percentage (%) of air parcels between isentropic surfaces of 360–420 K from MPTRAC simulations for the Nabro eruption. The percentage of air parcels are shown during **a** 12–30 June 2011, **b** 1–10 July 2011, **c** 11–20 July 2011, and **d** 21–30 July 2011. The bin size is $2^\circ \times 1^\circ$. The boundary of the ASMA is marked by the 14,320 m geopotential height at the 150 hPa pressure level (thick black contours). The filled red triangles indicate the Nabro volcano.

monotonously in the UTLS region, indicating that the diabatic heating rate in the ASMA was positive, and the altitude of the plume started to increase monotonously after the first 15 days. Based on the median values, the increase rate of the potential temperature, which is also the diabatic heating rate, was ~ 0.8 K per day. This slow upward transport in the ASMA has also been addressed in previous studies^{31,33}. Thus, volcanic gases and aerosols in the upper troposphere in the ASMA can be further elevated to the stratosphere over the ASMA. Moreover, as shown in ref. ³⁴, the air masses at the top of the ASMA will be further transported to the tropical stratosphere quasi-horizontally and enter the tropical pipe. Therefore, the ASMA plays a significant role in lifting volcanic plumes and expanding the influence of volcanic eruptions.

For the Sarychev eruption, the volcanic plume of the Sarychev eruption was mostly isolated outside of the ASM region, so the transport was not influenced by the diabatic heating. Most of the Sarychev volcanic plumes that were injected into the mid-latitude lower stratosphere and were transported quasi-horizontally to the TTL by ASMA circulation (as seen in Fig. 3) will undergo diabatic ascent due to the radiative heating there³⁵. This vertical transport is not directly related to the ASM region but is significantly facilitated by ASMA circulation.

As to the SO_2 emissions injected into the troposphere, we examined the transport process and found that only a small fraction of the volcanic plume that started right below the mid-latitude tropopause could end in the tropical stratosphere. The vertical transport was also forced by the radiative heating in the TTL, which is not directly associated with the ASM region either. More details are in the Supplementary information.

DISCUSSION

In this study, we retrieved the SO_2 emissions from the Sarychev eruption (2009) and Nabro eruption (2011) and investigated the transport of the volcanic plume in a realistic scenario under the influence of the ASM.

Conventionally, a tropical volcanic eruption, such as the Nabro eruption, receives more attention because it could inject SO_2 and sulfate aerosol directly into the tropical UTLS, where the upward branch of the Brewer–Dobson circulation spreads the aerosol over the globe and causes long-term climate effects. In contrast, an extratropical volcanic eruption, such as the Sarychev eruption, is usually thought to only have limited regional impacts because the SO_2 and sulfate aerosol injected into the extratropical UTLS would encounter the downward branch of the Brewer–Dobson circulation and be eliminated from the stratosphere.

As demonstrated above, even though most of the volcanic aerosols from the Sarychev eruption remained in the middle and high latitudes, a small but significant part of the aerosols was transported quasi-horizontally to the tropical UTLS by the ASMA. This meridional aerosol transport significantly enhanced the aerosol loading in the tropical stratosphere (also found in ref. ¹²). In these scenarios, the volcanic aerosol from a middle-latitude volcanic eruption could enter the Brewer–Dobson circulation and spread to the stratosphere of both hemispheres. In this case, it may impact global atmospheric radiation, similar to a tropical volcanic eruption. However, as a transport barrier, the ASMA generally prevented volcanic aerosols from entering the anticyclone, resulting in an aerosol hole over the ASMA in the UTLS region.

The boundary of the ASMA was initially defined by Randel and Park¹⁵ using the GPH of 14,320 m on the 150 hPa pressure level

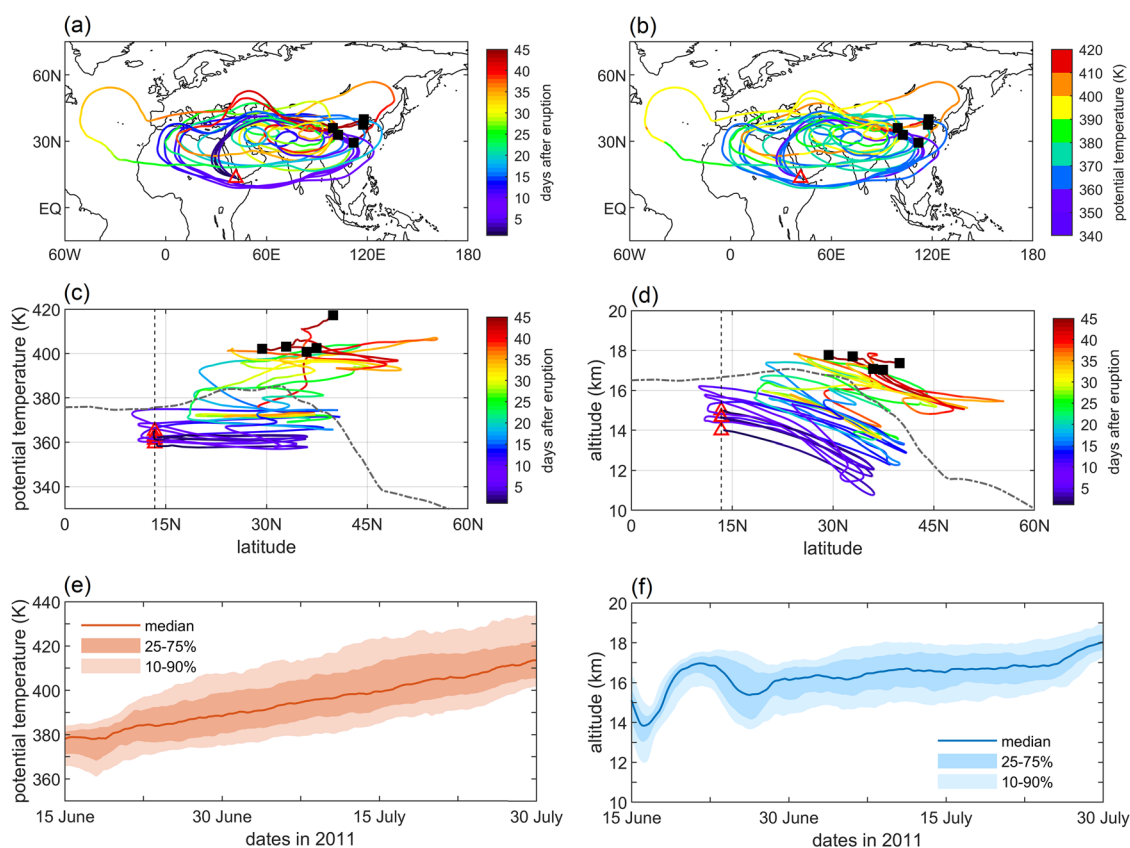


Fig. 5 Evolution of the attributes of the forward trajectories. Selected forward trajectories colored by **a** the days after 12 June 2011 and **b** the potential temperature (PT, unit: K) of the air parcels. **c** The latitude versus PT cross-sections of the forward trajectories and **d** the latitude versus altitude cross-sections colored by days after 12 June 2011. The open red triangles and the filled black squares indicate the starting and end locations of the selected air parcels, respectively. The vertical gray dashed line indicates the latitude of the Nabro volcano. The gray dot-dashed lines in **(c)** and **(d)** show the PT and altitude of the tropopause, respectively. The evolution of the altitude **(e)** and PT **(f)** of the air parcels elevated from the upper troposphere to the lower stratosphere within the ASMA. The solid line indicates the median value. The dark shading indicates the range of the 25th–75th percentiles, and the light shading indicates the range of the 10th–90th percentiles.

that roughly represents the streamline near the maximum wind speed in the upper troposphere, corresponding to an area featuring steep trace gases gradients (high tropospheric trace gases, e.g., CO and H₂O, and low stratospheric trace gases, e.g., O₃). As to the transport barrier effect of the ASMA, a PV-based boundary is more physically reasonable³². In the layered two-dimensional PV-conserving flows, the displacement of PV isolines is smaller in a strong PV-gradient background than in a weak PV background due to pseudomomentum conservation³⁶. The smaller displacement of PV isolines means less Rossby wave breaking and hence less transport, so regions of enhanced PV gradients indicate the transport barriers³⁷. The ASMA region is characterized by negative and anomalously low PV and enhanced PV gradients at its boundary, so this PV-gradient barrier initially applied to the transport barrier of the polar vortex^{38–40} can also explain the barrier effect associated with the ASMA.

In addition, the ASMA is bounded by the subtropical westerlies in the north and the tropical easterlies in the south (see Fig. 2). These zonal jets may inhibit meridional transport by increasing the intrinsic phase speed of Rossby waves, thereby suppressing Rossby wave breaking. This mechanism has been proved with model experiments^{37,41}, and the meridional transport barrier effect is verified to be true even for the subtropical jet in the boreal summer. So these zonal jets may contribute to the barrier effect in the north and south of the ASMA, respectively, independent of the PV gradients. The barrier effect caused by

the summer subtropical jets can also be explained by the effective diffusivity mixing diagnostics⁴².

For the Nabro eruption (2011), the ASMA transported most volcanic aerosol from the tropics to the middle latitudes. The aerosol was first confined in the ASMA in the UTLS region and then slowly leaked toward the northeast and southwest. Bourassa et al.⁴ argued that the Nabro eruption (2011) injected volcanic gases below the tropopause, and only via the ASM could the volcanic gases and aerosols ascend to the stratosphere, which raised broad discussions and some disagreements^{27,28}. Our study found that during the major eruption period (12–13 June 2011), the Nabro eruption injected part of the volcanic gases and aerosols directly into the lower stratosphere without the help of the ASM. Our study also found the volcanic plume injected into the upper troposphere was lifted in anticyclonic upward spirals, and during the troposphere-to-stratosphere ascent, the potential temperature level increased by ~0.8 K per day. With the isentropic surface of 360 K at 15.5 km and 420 K at 18.5 km³⁵, an uplift of 1 km means an increase of potential temperature by about 20 K. The ascent ratio of 0.8 K from this study results in an uplift of 1 km (20 K) in about 25 days due to radiative heating, which generally agrees with the radiative heating value previously deduced from observations⁷ and model simulations³¹. But Bourassa et al.⁴ showed an uplift of 40 K in 12 days (from 380 K on 13 June 2011 to 420 K on 25 June 2011). The ascent ratio of 40 K in 12 days is far beyond being explainable by radiative heating. The SO₂ and sulfate aerosols injected into the troposphere were elevated to the

stratosphere over the ASMA, from which they may further migrate to the tropical pipe. In this case, an altitude-resolved SO₂ emission inventory is necessary to accurately simulate the ASMA's influence on plume transport.

In summary, based on the transport study of volcanic plumes under the influence of the ASM, we found that ASMA can significantly increase the meridional transport between the tropical and extratropical UTLS. At the same time, the ASMA modulates the horizontal distribution of volcanic gases and aerosols due to its barrier effect. The ASMA also plays a significant role in troposphere-to-stratosphere vertical transport, which may increase the stratospheric loading of volcanic aerosols and expand the potential impacts of volcanic eruptions.

METHOD

Reanalysis data and satellite measurements

ERA5 is the fifth generation of reanalysis data from the European Centre for Medium-Range Weather Forecasts (ECMWF)⁴³. We retrieved the hourly and monthly averaged data with horizontal grids of 0.25° × 0.25° and the heights covering from 1000 to 1 hPa at 37 pressure levels to calculate the daily and monthly average of the range of the ASMA and calculate diagnostic parameters, such as potential temperature, potential vorticity, and tropopause.

ERA-Interim reanalysis data⁴⁴ is also provided by the ECMWF. Data on 1° × 1° horizontal grids from the surface to 0.1 hPa at 60 model levels were retrieved to drive the Lagrangian particle dispersion model. The ERA-Interim data are available 6-h at 00, 06, 12, and 18 UTC.

Atmospheric infrared sounder (AIRS) observations of SO₂ are used to initialize and evaluate the Lagrangian transport simulations. AIRS is an infrared sounder on the Aqua satellite launched in May 2002⁴⁵ and orbits in a nearly polar, sun-synchronous orbit at an altitude of ~710 km and a period of 98 min. Each across-track scan covers a ground distance of 1780 km and has 90 footprints. The footprint size varies between 13.5 km × 13.5 km at the nadir and 21.4 km × 41 km at the scan extremes. AIRS provides 14.5 orbits per day, covering the Earth approximately twice a day.

Volcanic eruptions of SO₂ are detected from AIRS measurements using the brightness temperature (BT) difference method. The SO₂ index (SI) is defined as the BT difference in the 7.3 μm waveband:

$$SI = BT(1412.87 \text{ cm}^{-1}) - BT(1371.52 \text{ cm}^{-1})$$

This definition improves the SI over the previous definition^{12,46} through a better choice of background channel (selecting 1412.87 cm⁻¹ rather than 1407.2 cm⁻¹). Moreover, this new SI is more sensitive to low concentrations and performs better in suppressing background interfering noise. The AIRS SI is most sensitive to SO₂ at altitudes in the UTLS region (8–13 km) and increases with increasing SO₂ column density. In this study, 4 K was set as the threshold, i.e., SI values greater than the threshold were identified as volcanic SO₂ emissions.

MPTRAC model

The transport and dispersion of volcanic plumes are simulated with the Massive-Parallel Trajectory Calculations model (MPTRAC) Version 2.2. MPTRAC is a Lagrangian particle dispersion model (LPDM) suitable for analyzing transport processes in the troposphere and stratosphere^{47,48}. It uses wind fields from reanalyzed data to calculate the trajectories of particles by solving the kinematic equation of motion. Additionally, the model includes subgrid-scale wind fluctuations and turbulent diffusion modules. Subgrid-scale wind fluctuations were simulated using the Langevin equation. The turbulent diffusion is described by a fixed diffusion coefficient. In this study, a constant horizontal diffusion

coefficient of 50 m² s⁻¹ was set for the troposphere, and a vertical diffusion coefficient of 0.1 m² s⁻¹ was set for the stratosphere. The MPTRAC Version 2.2 added modules to simulate the effects of convection, sedimentation, dry deposition, wet deposition, and hydroxyl chemistry on the depletion of SO₂ and aerosols⁴⁷. MPTRAC Version 2.2 significantly improved the simulations of the evolution of SO₂ and sulfate aerosols and produced more physically and chemically reasonable results compared with its older versions^{12,48}. The MPTRAC model has been used in several studies to simulate the long-range transport of volcanic SO₂ and sulfate aerosols^{12,49,50}.

In this study, the MPTRAC model was driven with the ERA-Interim wind field, which gives the optimized balance between computational costs and accuracy^{48,51}.

Method of reconstructing volcanic SO₂ emission time series

The SO₂ emissions from the two volcanic eruptions, Sarychev (2009) and Nabro (2011), and the subsequently converted sulfate aerosols were used as “realistic” tracers to investigate the influence of the ASM on transporting the erupted materials. The method of reconstructing the time series of the mass and plume height of the injected SO₂ follows the basic ideas of ref.⁴⁸, which uses AIRS SO₂ measurements and backward trajectories.

Because AIRS only provides column density measurements without altitude-resolved information, we set up a column at each location of the AIRS SO₂ measurements (SO₂ index). The altitude range of the column was 0–30 km, which may cover the vertical dispersion range of the SO₂ plume during the eruption period. A total number of 100,000 air parcels was assigned to all the columns, and the number of air parcels in each column was weighted according to the SO₂ index, and the vertical distribution of the air parcels in each column followed the mean kernel function of the AIRS SO₂ measurements. The AIRS footprint size is between 13.5 and 41 km, so in the horizontal plane, we chose 30 km as the full width at half maximum (FWHM) for the horizontal Gaussian scatter of the air parcels. Then, backward trajectories were calculated for all air parcels. SO₂ trajectories that were at least one day and up to 7 days and had passed the volcano domain were considered SO₂ emissions of the volcanic eruptions. The volcano domain was within a radius of 75 km from the volcanoes and a vertical range of 0–25 km, covering the injection height. These preassigned parameters were selected with sensitivity experiments to optimize to obtain the best simulation results.

This approach retrieves the realistic spatial and temporal distributions of SO₂ emissions but requires the total mass of SO₂ from additional datasets⁴⁸. Following estimations from previous studies^{52–55} and the Global Volcanism Program reports^{23,24}, a total SO₂ mass of 1.4 Tg and 3.65 Tg was assigned to the Sarychev and Nabro eruptions, respectively. This approach was successfully used in reverse modeling of volcanic SO₂ emissions of multiple volcanic eruptions^{12,33,48–50}.

DATA AVAILABILITY

The SO₂ index data used in this study are available for download at <https://datapub.fz-juelich.de/slcs/airs/volcanoes/> (last access: 30 June 2022). The MIPAS aerosol index data used in this study are available for download at https://datapub.fz-juelich.de/slcs/mipas/aerosol_clouds/ (last access: 21 July 2022). The ERA-Interim reanalysis data were obtained from the European Centre for Medium-Range Weather Forecasts (ECMWF). The ERA5 reanalysis data were retrieved from ECMWF Meteorological Archival and Retrieval System (<https://doi.org/10.24381/cds.adbb2d47> last accessed: 15 June 2022).

CODE AVAILABILITY

The code of the Massive-Parallel Trajectory Calculations (MPTRAC) model is available under the terms and conditions of the GNU General Public License, Version 3 from

the repository at <https://github.com/slcs-jsc/mptrac> (last access: 25 August 2021). The codes developed to analyze the data of the study and produce the figures are available from the corresponding authors on request.

Received: 17 August 2022; Accepted: 8 February 2023;

Published online: 21 February 2023

REFERENCES

- Hofmann, D., Barnes, J., O'Neill, M., Trudeau, M. & Neely, R. Increase in background stratospheric aerosol observed with lidar at Mauna Loa Observatory and Boulder, Colorado. *Geophys. Res. Lett.* **36**, L15808 (2009).
- Solomon, S. et al. The persistently variable "background" stratospheric aerosol layer and global climate change. *Science* **333**, 866–870 (2011).
- Vernier, J. P. et al. Major influence of tropical volcanic eruptions on the stratospheric aerosol layer during the last decade. *Geophys. Res. Lett.* **38**, L12807 (2011).
- Bourassa, A. E. et al. Large volcanic aerosol load in the stratosphere linked to Asian monsoon transport. *Science* **337**, 78–81 (2012).
- Kloss, C. et al. Stratospheric aerosol layer perturbation caused by the 2019 Raikoke and Ulawun eruptions and their radiative forcing. *Atmos. Chem. Phys.* **21**, 535–560 (2021).
- Vaughan, G., Wareing, D. & Ricketts, H. Measurement report: lidar measurements of stratospheric aerosol following the 2019 Raikoke and Ulawun volcanic eruptions. *Atmos. Chem. Phys.* **21**, 5597–5604 (2021).
- Fairlie, T. D., Vernier, J. P., Natarajan, M. & Bedka, K. M. Dispersion of the Nabro volcanic plume and its relation to the Asian summer monsoon. *Atmos. Chem. Phys.* **14**, 7045–7057 (2014).
- Andersson, S. M. et al. Significant radiative impact of volcanic aerosol in the lowermost stratosphere. *Nat. Commun.* **6**, 7692 (2015).
- Yu, P., Toon, O. B., Neely, R. R., Martinsson, B. G. & Brenninkmeijer, C. A. M. Composition and physical properties of the Asian Tropopause Aerosol Layer and the North American Tropospheric Aerosol Layer. *Geophys. Res. Lett.* **42**, 2540–2546 (2015).
- Bian, J. et al. Transport of Asian surface pollutants to the global stratosphere from the Tibetan Plateau region during the Asian summer monsoon. *Natl. Sci. Rev.* **7**, 516–533 (2020).
- Konopka, P., Groöf, J.-U., Plöger, F. & Müller, R. Annual cycle of horizontal in-mixing into the lower tropical stratosphere. *J. Geophys. Res. Atmos.* **114**, D19111 (2009).
- Wu, X., Griessbach, S. & Hoffmann, L. Equatorward dispersion of a high-latitude volcanic plume and its relation to the Asian summer monsoon: a case study of the Sarychev eruption in 2009. *Atmos. Chem. Phys.* **17**, 13439–13455 (2017).
- Kloss, C. et al. Transport of the 2017 Canadian wildfire plume to the tropics via the Asian monsoon circulation. *Atmos. Chem. Phys.* **19**, 13547–13567 (2019).
- Zarrin, A., Ghaemi, H., Azadi, M. & Farajzadeh, M. The spatial pattern of summertime subtropical anticyclones over Asia and Africa: A climatological review. *Int. J. Climatol.* **30**, 159–173 (2010).
- Randel, W. J. & Park, M. Deep convective influence on the Asian summer monsoon anticyclone and associated tracer variability observed with Atmospheric Infrared Sounder (AIRS). *J. Geophys. Res. Atmos.* **111**, D12314 (2006).
- Randel, W. J. et al. Asian monsoon transport of pollution to the stratosphere. *Science* **328**, 611–613 (2010).
- Vogel, B. et al. Long-range transport pathways of tropospheric source gases originating in Asia into the northern lower stratosphere during the Asian monsoon season 2012. *Atmos. Chem. Phys.* **16**, 15301–15325 (2016).
- Vogel, B., Guenther, G., Mueller, R., Grooss, J. U. & Riese, M. Impact of different Asian source regions on the composition of the Asian monsoon anticyclone and of the extratropical lowermost stratosphere. *Atmos. Chem. Phys.* **15**, 13699–13716 (2015).
- Santee, M. L. et al. A comprehensive overview of the climatological composition of the Asian summer monsoon anticyclone based on 10 years of Aura Microwave Limb Sounder measurements. *J. Geophys. Res. Atmos.* **122**, 5491–5514 (2017).
- Tissier, A. S. & Legras, B. Convective sources of trajectories traversing the tropical tropopause layer. *Atmos. Chem. Phys.* **16**, 3383–3398 (2016).
- Fadnavis, S. et al. The impact of recent changes in Asian anthropogenic emissions of SO₂ on sulfate loading in the upper troposphere and lower stratosphere and the associated radiative changes. *Atmos. Chem. Phys.* **19**, 9989–10008 (2019).
- Fadnavis, S. et al. Transport of aerosols into the UTLS and their impact on the Asian monsoon region as seen in a global model simulation. *Atmos. Chem. Phys.* **13**, 8771–8786 (2013).
- Global Volcanism Program. Report on Sarychev Peak (Russia). *BGVN* **34**, 6 (2009).
- Global Volcanism Program. Report on Nabro (Eritrea). *BGVN* **36**, 9 (2011).
- Levin, B. W. et al. Monitoring of the eruption of the Sarychev Peak Volcano in Matua Island in 2009 (central Kurile islands). *Dokl. Earth Sci.* **435**, 1507–1510 (2010).
- Rybin, A. et al. Satellite and ground observations of the June 2009 eruption of Sarychev Peak volcano, Matua Island, Central Kuriles. *Bull. Volcanol.* **73**, 1377–1392 (2011).
- Fromm, M., Nedoluha, G. & Charvat, Z. Comment on "large volcanic aerosol load in the stratosphere linked to Asian monsoon transport". *Science* **339**, 2 (2013).
- Vernier, J.-P. et al. Comment on "large volcanic aerosol load in the stratosphere linked to Asian monsoon transport". *Science* **339**, 647–647 (2013).
- Garny, H. & Randel, W. J. Dynamic variability of the Asian monsoon anticyclone observed in potential vorticity and correlations with tracer distributions. *J. Geophys. Res. Atmos.* **118**, 13421–13433 (2013).
- Vogel, B. et al. Fast transport from Southeast Asia boundary layer sources to northern Europe: rapid uplift in typhoons and eastward eddy shedding of the Asian monsoon anticyclone. *Atmos. Chem. Phys.* **14**, 12745–12762 (2014).
- Vogel, B. et al. Lagrangian simulations of the transport of young air masses to the top of the Asian monsoon anticyclone and into the tropical pipe. *Atmos. Chem. Phys.* **19**, 6007–6034 (2019).
- Ploeger, F. et al. A potential vorticity-based determination of the transport barrier in the Asian summer monsoon anticyclone. *Atmos. Chem. Phys.* **15**, 13145–13159 (2015).
- Zhang, J. et al. Aerosol variations in the upper troposphere and lower stratosphere over the Tibetan Plateau. *Environ. Res. Lett.* **15**, 094068 (2020).
- Garny, H. & Randel, W. J. Transport pathways from the Asian monsoon anticyclone to the stratosphere. *Atmos. Chem. Phys.* **15**, 25981–26023 (2016).
- Fueglistaler, S. et al. Tropical tropopause layer. *Rev. Geophys.* **47**, 31 (2009).
- Shepherd, T. G. Rigorous bounds on the nonlinear saturation of instabilities to parallel shear flows. *J. Fluid Mech.* **196**, 291–322 (1988).
- Beron-Vera, F. J., Olascoaga, M. J., Brown, M. G. & Kocak, H. Zonal jets as meridional transport barriers in the subtropical and polar lower stratosphere. *J. Atmos. Sci.* **69**, 753–767 (2012).
- Butchart, N. & Remsburg, E. E. The area of the stratospheric polar vortex as a diagnostic of tracer transport on an isentropic surface. *J. Atmos. Sci.* **43**, 1319–1339 (1986).
- Manney, G. L., Zurek, R. W., Gelman, M. E., Miller, A. J. & Nagatani, R. The anomalous Arctic lower stratospheric polar vortex of 1992–1993. *Geophys. Res. Lett.* **21**, 2405–2408 (1994).
- Nash, E. R., Newman, P. A., Rosenfield, J. E. & Schoeberl, M. R. An objective determination of the polar vortex using Ertel's potential vorticity. *J. Geophys. Res. Atmos.* **101**, 9471–9478 (1996).
- Rypina, I. I., Brown, M. G. & Beron-Vera, F. J. On the lagrangian dynamics of atmospheric zonal jets and the permeability of the stratospheric polar vortex. *J. Atmos. Sci.* **64**, 3595–3610 (2007).
- Haynes, P. & Shuckburgh, E. Effective diffusivity as a diagnostic of atmospheric transport: 2. Troposphere and lower stratosphere. *J. Geophys. Res. Atmos.* **105**, 22795–22810 (2000).
- Hersbach, H. et al. The ERA5 global reanalysis. *Q. J. R. Meteorol. Soc.* **146**, 1999–2049 (2020).
- Dee, D. P. et al. The ERA-Interim reanalysis: configuration and performance of the data assimilation system. *Q. J. R. Meteorol. Soc.* **137**, 553–597 (2011).
- Aumann, H. H. et al. AIRS/AMSU/HSB on the Aqua mission: design, science objectives, data products, and processing systems. *IEEE Trans. Geosci. Remote Sens.* **41**, 253–264 (2003).
- Hoffmann, L., Griessbach, S. & Meyer, C. I. Volcanic emissions from AIRS observations: detection methods, case study, and statistical analysis. In *Proc. Remote Sensing of Clouds and the Atmosphere XIX and Optics in Atmospheric Propagation and Adaptive Systems XVII* (eds Cameron, A. et al.) **9242**, 305–312 (International Society for Optics and Photonics, 2014).
- Hoffmann, L. et al. Massive-parallel trajectory calculations version 2.2 (MPTRAC-2.2): Lagrangian transport simulations on graphics processing units (GPUs). *Geosci. Model. Dev.* **15**, 2731–2762 (2022).
- Hoffmann, L., Rößler, T., Griessbach, S., Heng, Y. & Stein, O. Lagrangian transport simulations of volcanic sulfur dioxide emissions: Impact of meteorological data products. *J. Geophys. Res. Atmos.* **121**, 4651–4673 (2016).
- Wu, X., Griessbach, S. & Hoffmann, L. Long-range transport of volcanic aerosol from the 2010 Merapi tropical eruption to Antarctica. *Atmos. Chem. Phys.* **18**, 15859–15877 (2018).
- Cai, Z., Griessbach, S. & Hoffmann, L. Improved estimation of volcanic SO₂ injections from satellite retrievals and Lagrangian transport simulations: the 2019 Raikoke eruption. *Atmos. Chem. Phys.* **22**, 6787–6809 (2022).
- Hoffmann, L. et al. From ERA-Interim to ERA5: the considerable impact of ECMWF's next-generation reanalysis on Lagrangian transport simulations. *Atmos. Chem. Phys.* **19**, 3097–3124 (2019).

52. Clarisse, L. et al. Retrieval of sulphur dioxide from the infrared atmospheric sounding interferometer (IASI). *Atmos. Meas. Tech.* **5**, 581 (2012).
53. Haywood, J. M. et al. Observations of the eruption of the Sarychev volcano and simulations using the HadGEM2 climate model. *J. Geophys. Res. Atmos.* **115**, D21212 (2010).
54. Jégou, F. et al. Stratospheric aerosols from the Sarychev volcano eruption in the 2009 Arctic summer. *Atmos. Chem. Phys.* **13**, 6533–6552 (2013).
55. Theys, N. et al. Volcanic SO₂ fluxes derived from satellite data: a survey using OMI, GOME-2, IASI and MODIS. *Atmos. Chem. Phys.* **13**, 5945–5968 (2013).

ACKNOWLEDGEMENTS

This study is supported by the National Natural Science Foundation of China (Grants 41975049, 42175046, 42065009, 41861134034, and 41905042). X Wu is also supported by the Basic Strengthening Research Program (Grant 2021-JCJQ-JJ-1058), and the Ground-based Space Environment Comprehensive Monitoring Network (the Chinese Meridian Project II). B Chen is supported by the Natural Science Foundation of Yunnan Province (Grant 201901BB050045). X Wang is supported by the Strategic Priority Research Program of the Chinese Academy of Sciences (Grant XDA15021000). L Hoffmann is supported by the joint research project AeroTrac of the Deutsche Forschungsgemeinschaft (Grant DFG HO5102/1-1). YF Tian is supported by the Open Research Project of Large Research Infrastructures of CAS—“Study on the interaction between low/mid-latitude atmosphere and ionosphere based on the Chinese Meridian Project”. YN Wang is supported by the second Tibetan Plateau Scientific Expedition and Research Program (Grant 2019QZKK0604).

AUTHOR CONTRIBUTIONS

X. Wu and X. Wang developed the idea. All the authors discussed the concepts. X. Wu, Q.Q., and B.C. performed most of the analysis. X. Wu drafted the manuscript and all authors edited and revised the manuscript. All authors approved the completed version of the manuscript.

COMPETING INTERESTS

The authors declare no competing interests.

ADDITIONAL INFORMATION

Supplementary information The online version contains supplementary material available at <https://doi.org/10.1038/s41612-023-00339-w>.

Correspondence and requests for materials should be addressed to Bing Chen or Xin Wang.

Reprints and permission information is available at <http://www.nature.com/reprints>

Publisher's note Springer Nature remains neutral with regard to jurisdictional claims in published maps and institutional affiliations.



Open Access This article is licensed under a Creative Commons Attribution 4.0 International License, which permits use, sharing, adaptation, distribution and reproduction in any medium or format, as long as you give appropriate credit to the original author(s) and the source, provide a link to the Creative Commons license, and indicate if changes were made. The images or other third party material in this article are included in the article's Creative Commons license, unless indicated otherwise in a credit line to the material. If material is not included in the article's Creative Commons license and your intended use is not permitted by statutory regulation or exceeds the permitted use, you will need to obtain permission directly from the copyright holder. To view a copy of this license, visit <http://creativecommons.org/licenses/by/4.0/>.

© The Author(s) 2023